Aerosol radiative forcings induced by variations in anthropogenic emissions over China during 2008–2016

Mingxu Liu[1] and Hitoshi Matsui[1]

[1]Graduate School of Environmental Studies, Nagoya University, Nagoya, Japan

Corresponding to: Hitoshi Matsui (matsui@nagoya-u.jp)

Abstract. Anthropogenic emissions in China play an important role in altering global radiation budget. Over the recent decade, the clean-air options in China resulted in substantial reductions in anthropogenic emissions, such as sulfur dioxide (SO_2) and primary carbonaceous aerosols, and consequently improved air quality. However, the resultant aerosol radiative forcings are poorly understood and few reported. In this study, we use an advanced global climate model integrated with the latest anthropogenic emission inventory to estimate the aerosol radiative forcings by the anthropogenic emission variation in China between 2008 and 2016. Our simulations exhibit decreases of 46% and 25% for the annual mean surface-level sulfate and black carbon (BC) mass concentrations in East China, respectively, which is the key region subject to stringent emission control options. In the meantime, the simulated aerosol optical depth and aerosol absorption optical depth show decreasing tendencies. Results reveal that the substantial reduction in SO_2 emissions yields a positive all-sky shortwave direct radiative forcing of +0.17 W m^{-2} at the top of the atmosphere (TOA) in East China during 2008–2016 primarily through the weakening of sulfate scattering effects, as well as an aerosol-induced cloud radiative forcing of +0.13 W m^{-2}. The concurrent reduction in BC emissions induces a negative BC radiative forcing of −0.34 W m^{-2}. Hence, the positive radiative forcing by the SO_2 emission reductions may be counterbalanced by those decreases of BC concentrations in China during 2008–2016. Besides, the model experiments show a clear enhancement of the downward solar radiation flux that reach the Earth's surface over China caused by the mitigation of aerosol pollution, agreeing with long-term observation records of the shortwave energy balance from other studies. While the radiative forcing at TOA is small locally due to the counteracted effects of SO_2 and BC emissions, it is relatively larger (+0.16 W m^{-2}) over the downwind north Pacific region, mainly induced by the reductions in sulfate particles and their effects on cloud properties. By adopting comprehensive future emission scenario for China in 2030 and 2050 developed by the recent study, we predict that the strictest environmental policies will induce the change of aerosol radiative forcings of +0.55 and +1.23 W m^{-2} over East China between 2016−2030 and 2016−2050, respectively. Since aerosol radiative forcings potentially influence surface temperature, boundary layer dynamics, and precipitation through fast climate responses, tailored emission control policies are desirable to improve air quality and mitigate the risk of climate change in the future.

1. Introduction

Aerosols perturb the global energy balance by aerosol-radiation interactions, such as the scattering and absorption of sunlight (Charlson et al., 1992), and by aerosol-cloud interactions through the activation of cloud condensation nuclei (CCN) particles into cloud droplets, which impact on both the cloud albedo and lifetime (Twomey, 1974; Andreae and Rosenfeld, 2008). The changes in anthropogenic aerosol concentrations from preindustrial to present days are estimated to induce a global-mean net cooling effect of −0.4 to −1.5 W m^{-2} at the top of the atmosphere (TOA) that partly masks the warming effects by increased carbon dioxide (Boucher et al., 2013).

It is commonly known that black carbon (BC) and sulfate aerosols are important contributors to the radiation absorption and scattering effects of anthropogenic aerosols in the global scale. Bond et al. (2013) estimated that the industrial-era (1750−2005) direct radiative forcing (DRF) of BC is 0.71 W m^{-2}. Until now, uncertainties embedded in the radiative forcing (RF) of BC are still large due to the insufficient treatment of BC atmospheric processes in climate models including the impacts of BC on liquid clouds (Koch and Del Genio, 2010; Chung and Seinfeld, 2002) and the role of BC in acting as ice nuclei (Kulkarni et al., 2016). Moreover, the mixing state is one of the key parameters that determine the optical properties and CCN activity of BC (Jacobson, 2001; Stier et al., 2006; Matsui, 2016). Recent studies find that explicit representation of BC aging processes can increase the confidence in the estimates of BC DRF (Matsui et al., 2018a). Unlike BC that is directly emitted into the atmosphere, sulfate aerosols mainly originate from the chemical transformation of sulfur dioxide (SO_2) via the photochemical oxidation by OH radical, aqueous and heterogeneous reactions (Seinfeld and Pandis, 2016). The estimates of sulfate radiative forcings rely heavily on the representation of secondary sulfate formation in climate models and SO_2 emissions (Huang et al., 2015). Sulfate aerosols are estimated to exert a global-mean DRF of −0.32 W m^{-2} for the time period of 1750 to 2010 (Myhre et al., 2013), with remarkable radiative perturbation in the north mid-latitude region (20 °–40 °N) due to the rapidly increased anthropogenic SO_2 emissions in China over the past few decades. The tremendous anthropogenic emissions in China not only result in severe air pollution, but also significantly alter the global shortwave radiation budget (Li et al., 2016a).

During the past ten years, China has implemented stringent air pollution control measures and the SO_2 emissions started to decrease in 2007 with the application of flue gas desulfurization in the power sector. Especially since 2013, the toughest-ever clean air policies have led to substantial reductions in anthropogenic emissions in China. According to the latest emission inventory, the national annual emissions of SO_2, nitrogen oxides (NO_x), BC, and organic carbon (OC) have declined by 62%, 17%, 27%, and 35%, respectively during 2010−2017 (Zheng et al., 2018). Recent studies have demonstrated significant improvements of air quality in China attributable to those various emission control measures (Zhang et al., 2019). Specifically, SO_2 emissions exhibited the most notable reduction among all pollutants for this period, which reduce the concentrations of sulfate aerosols dramatically and mitigate the $PM_{2.5}$ pollution and acid rain issues (Liu et al., 2020; Liu et al., 2018).

The unprecedented reductions in anthropogenic emissions over China provide a unique opportunity to investigate the responses of aerosol climate effects to such considerable variations in precursor emissions. Those emissions changes would lead to the

perturbation of regional solar radiation budgets, mainly reflected by the aerosol forcings at the top of atmosphere due to aerosol-radiation interactions and aerosol-cloud interactions. Fadnavis et al. (2019) estimate that the Chinese SO_2 emissions reduction during 2006–2017 produces a positive clear-sky direct radiative forcing of +0.6 to +6 W m^{-2} over China. Paulot et al. (2018) have investigated the trends in the aerosol radiative effects in eastern China from 2001 to 2015 and shown a clear decreasing tend in AOD starting from 2007 due to reductions in SO_2 emissions. We find that previous estimates of aerosol forcings may be inadequate since they adopt a clear-sky condition and simple treatment of the mixing between sulfate and BC and do not consider the aerosol-cloud interaction in their simulations, all of which are important in the calculation of aerosol total radiative effects (Ghan, 2013). Until now, it remains unclear how the overall changes in anthropogenic emissions in China in the past decade (from 2007 to the present) including not only SO_2 emissions but also BC and other aerosol components impact aerosol forcings in source regions and outflows. BC emissions are reported to be significantly reduced in eastern China from 2010 to 2019 as inferred from rapidly decreased BC concentrations observed at an in-situ site near China mainland (Kanaya et al., 2020). Because BC particles exert a positive radiative effect through direct absorption of solar radiation and absorption enhancement by non-BC particles (like sulfate and organics) in the atmosphere (Matsui, 2020), the radiative effects caused by the changes in BC and non-BC emissions should be quantified in detail. Estimates of aerosol radiative forcings can favor a better prediction of the climate responses of future emission scenarios, like the shared-economic pathways (SSPs), on a regional or global scale.

In this study, we aim to evaluate the response of aerosol RFs consisting of direct radiative forcings and aerosol effects on clouds to the changes in anthropogenic emissions in China between 2008 and 2016. We chose this period for analysis because the differences of emissions between these two years (2008 and 2016) can reflect the inter-annual changes in China's anthropogenic emissions caused by a series of national air pollution control measures conducted over the past decade (Li et al., 2017; Zhang et al., 2019). Model experiments using an advanced global climate model integrated with the latest bottom-up emission inventory for China are performed to diagnose the RFs from changes in different aerosol components (sulfate, nitrate, BC etc.) and their interactions with radiation and clouds. We further predict the aerosol RFs with projected emission scenarios for the years 2030 and 2050.

2. Methods

2.1 Model experiments

In this study, we use the Community Atmosphere Model version 5 (CAM5) with the Aerosol Two-dimensional bin module for foRmation and Aging Simulation version 2 (CAM5/ATRAS2) (Matsui and Mahowald, 2017; Matsui, 2017). The release version of CAM5 can simulate emissions, gas-phase chemistry (MOZART), aerosol microphysical and secondary formation processes, wet/dry deposition, and aerosol-radiation-cloud interactions (Liu et al., 2012). The ATRAS2 module (Matsui et al., 2014) uses a two-dimensional sectional representation with 12 particle size bins (from 1 to 10000 nm in diameter) and 8 BC

mixing state bins (from fresh BC to aged BC-containing particles) for various microphysical and chemical processes of aerosols, including new particle formation, condensation/coagulation, aerosol activation, wet/dry deposition, and interactions with radiation and clouds. The model treats aerosol–cloud interactions in stratiform clouds using a physically based two-moment parameterization that considers the aerosol effects on cloud properties (Morrison and Gettelman, 2008). The secondary formation of sulfate is found to be important when simulation sulfate concentrations in China, but is not represented well in current chemistry-climate models (Hung and Hoffmann, 2015; Cheng et al., 2016). To better reproduce the temporal evolution of sulfate concentrations in China, we add a new pathway suggested by previous studies for secondary sulfate formation in our model, that is, the heterogeneous oxidation of gaseous SO_2 to particulate sulfate onto aerosol surfaces under high humidity conditions (Huang et al., 2014). The uptake coefficients of SO_2 are specified as the range between 2.0×10^{-5} and 1.0×10^{-4} under the ambient relative humidity of 50−100%.

The model is running at the horizontal resolution of $1.9° \times 2.5°$ with 30 vertical layers from the surface to ~40 km on a global scale. Several simulation experiments are designed with different inputs of anthropogenic emissions as shown in Table 1. We vary the anthropogenic emissions of all species for years 2008 and 2016 in China, termed as Exp08 and Exp16, respectively. The Exp16SO2 and Exp16BC cases are made by replacing the SO_2 and BC emissions in the Exp08 with those for 2016, respectively. Note that the radiative effects of each aerosol component are calculated online by our model and we use the results in the Exp08-Exp16 cases for discussing the main conclusion and implications. The cases of Exp16SO2 and Exp16BC with only one of the emission change included are used for comparison with the Exp16 to reflect the feedback of BC and SO_2 emission variations. We perform 2-year simulations for each experiment and the first year is for spin-up and the second year is for analysis. The meteorological fields are nudged by using the Modern-Era Retrospective analysis for Research and Applications Version 2 (MERRA2) data and are fixed at the year 2008 in these experiments to separate the contribution of emissions on aerosol radiative effects from variation in meteorological fields. The inter-annual change in meteorological conditions could influence aerosol radiative forcings but is not the focus of this study, and we simply discuss their importance in Section 3.3.

We estimate both the direct radiative effects of aerosols (DRE) and cloud radiative effects (CRE) in the model. The changes in DRE and CRE between the emissions years 2008 and 2016 can be regarded as aerosol DRF and aerosol-induced cloud radiative forcing (CRF) owing to the variation of anthropogenic emissions. Specifically, the aerosol DRE at TOA for each specific aerosol component (e.g., sulfate, BC and others) is online calculated as the differences between the standard radiation fluxes and the diagnosed one that subtracts this species in the radiation module. Then the aerosol DRF is calculated as the difference of DRE between 2008 and 2016. The aerosol effects on clouds are diagnosed following Ghan (2013) using the variables of clean-sky (neglecting the scattering and absorption of all aerosol species) radiation flux. The CRF values are scaled offline to the best estimate (-0.5 W m^{-2}) of effective radiative forcing due to aerosol-cloud interactions given by the Fifth Assessment Report of the Intergovernmental Panel on Climate Change (IPCC AR5) (Boucher et al., 2013). This process yields

a reasonable estimate of CRF based on our model results and present knowledge of aerosol-cloud interactions from the latest IPCC report.

2.2 Anthropogenic emissions for China

The global anthropogenic emissions for the year of 2008 are taken from Hoesly et al. (2018) based on the Community Emissions Data System (CEDS), while the emissions in China are replaced by the Multi-resolution Emission Inventory (MEIC) for 2008 or 2016, which provide a more realistic representation of China's emissions from fossil fuels and biofuels (Zheng et al., 2018). The global emissions other than China used in all simulations are provided by the CEDS for 2008. In addition, the ammonia emissions in China are taken from Liu et al. (2018), in which the estimates of agricultural ammonia emissions are well constrained and show good performance in the simulation of atmospheric ammonia burdens. As shown in Table 2, several major species including BC, primary OC, and SO_2 from anthropogenic sources experience reductions of emissions between 2008 and 2016 due to the clean-air policy in China in this period. The majority (more than 90%) of those emission reductions are found in East China (marked in Fig. 1), which is characterized with dense population and economic activities and is the key region subject to stringent air pollution control. For instance, emission reductions in East China are 57% for SO_2, 27% for BC, and 30% for OC.

2.3 Observation data

In order to evaluate the model performance for aerosol simulations, we collect the monthly measurement concentrations of inorganic aerosol chemical components (sulfate, nitrate, and ammonium) from Acid Deposition Monitoring Network in East Asia (EANET). The database has been widely used for the studies of air pollution and acid deposition for the region (Itahashi et al., 2018). The EANET stations used in this study include one site in southern China and nine sites in western and central Japan (Table S1). We also obtain the observation data of aerosol compounds for the period 2008–2016 from different measurement campaigns and the yearly averages of them are used to indicate the decadal variation of major aerosol components over China (Table S1). For comparison, the annual mean simulation results are taken from the model surface-level horizontal grid closest to these observation sites. In addition, we use observations of vertical profiles of BC concentrations from the HIAPER Plow-to-Plow Observations (HIPPO) aircraft campaigns conducted in the north Pacific region (Wofsy, 2011). The HIPPO data are obtained from five deployments across the central Pacific during 2009−2011 and include measurements of BC mass concentrations from a single-particle soot photometer (SP2) instrument (Schwarz et al., 2013). The monthly mean BC concentrations in the simulation for 2008 are used for comparison with observations from the same month in five HIPPO campaigns despite the differences in the years selected between the model and observations (Fig. S1).

We employ measurements of aerosol optical depth (AOD) and single scatter albedo (SSA) from Aerosol Robotic Network (AERONET) stations to reflect variations of aerosol optical properties during 2008–2016. The available stations that have long-term data records are Beijing (39.98 °N, 116.38 °E) and Xianghe (39.75 °N, 116.96 °E). In addition, the AOD at 550 nm

retrieved by the Multi-angle Imaging Spectroradiometer (MISR) Level-3 product (Garay et al., 2020) and the dark target and deep blue combined 550 AOD by the Moderate Resolution Imaging Spectroradiometer (MODIS) aboard NASA's Terra (Sayer et al., 2014) are used for comparison with our model results. Both satellite products provide the annual-mean or monthly-mean AOD data at a horizontal resolution of 0.5 ° × 0.5 °that can reflect the temporal changes over China during 2008–2016.

3. Results

3.1 Changes in the burdens of sulfate and BC mass

We first evaluate the simulated sulfate mass concentrations with the observations in China and Japan between the emission years of 2008 and 2016 (Fig. 1a, b). The simulated sulfate concentrations using CAM5/ATRAS2 model generally agree with available observations with respect to the magnitude and spatial patterns, showing high annual mean concentrations up to 20 μg m^{-3} in East China in 2008 and decreasing to less than 10 μg m^{-3} in 2016 due to the reductions of about 60% in SO_2 emissions (Table S2). Greater reductions of more than 10 μg m^{-3} are found in northern part of East China (Fig. 1a, b), where the SO_2 reductions are the most notable in the country (Li et al., 2017). The observed SO_2 loadings given by Li et al. (2017) show severe SO_2 pollutions (up to 2.0 DU, 1 DU = 2.69 × 10^{16} molecules cm^{-2}) before 2010 in the northern China and significant mitigation in 2016 with the column reaching as low as about 0.5 DU. Despite the lack of sulfate monthly observations, the model satisfactorily captures the seasonal profiles of SO_2 amounts retrieved by the Aura Ozone Monitoring Instrument (Fig. S2). The variation of annual mean sulfate concentrations in East China is on average of −3.5 μg m^{-3} (−46%) from 2008 to 2016, which is close to another model result (−50%) within the region (Liu et al., 2018). The sulfate mass column burden (integral of concentrations from surface to the top of atmosphere) averaged over East China exhibits a decrease of 4.5 mg m^{-2}, equal to 35% of that in 2008 (Fig. 2a, c). Moreover, the sulfate burden in the northern Pacific (the region marked in Fig. 2) decreases on average by 0.38 mg m^{-2} (−18%), reflecting the impacts of SO_2 emission reductions from East China to the downwind regions dominated by the westerly wind field in the middle latitudes.

We verify the variation of modeled BC concentrations using the measurements in three typical sites located in East China and western Japan (Fig. 1c, d). The long-term observational records of BC concentrations in Beijing and Shanghai present clear decreasing trends over the recent decade (Xia et al., 2020; Wei et al., 2020). During 2008–2016, the annual mean surface BC decreases from 8.5 μg m^{-3} to 3.5 μg m^{-3} in Beijing, and from about 4.0 μg m^{-3} to 2.2 μg m^{-3} in Shanghai. Similar reductions are shown in our simulations for the emission years of 2008 and 2016, with the averaged decrease of 25% over East China. The continuous decline (−5.8±1.5) % yr^{-1}) in surface BC concentrations observed at Fukue Island in western Japan from 2010 to 2018 further supports the reduction of the BC emissions in East China (Kanaya et al., 2020). Moreover, we evaluate the vertical distributions of BC concentrations in the northern Pacific using the BC measurement by HIPPO campaigns (Fig. S1). Despite some underestimation of modeled BC in a few months, there is in general a reasonable agreement between modeled and observed BC concentrations from surface to the upper troposphere. During 2008–2016, the annual mean BC burdens

decrease by 0.38 mg m^{-2} (22%) in East China and by 0.016 mg m^{-2} (13%) in the northern Pacific, respectively (Fig. 2b, d). The results suggest that the integration of CAM5/ATRAS2 model and the MEIC emission inventory for China can reproduce the observed decline in the sulfate and BC concentrations over the recent decade caused by the variations of anthropogenic emissions.

The simulated particulate nitrate concentrations are compared well with the measurements (Fig. S3 and Table S2). We find that the annual mean nitrate concentrations are elevated by about 1.0 μg m^{-3} (20%) in East China between emission years 2008 (Exp08) and 2016 (Exp16). The nearly consistent variation takes place in the Exp16SO2 case. Since NH_3 emissions are unchanged, the variation in SO_2 emissions is responsible for the increases of particulate nitrate concentrations. This is because the reduction of ammonium sulfate particles releases free ammonia in the air and consequently facilitates the thermodynamic partitioning of nitrate toward the aerosol phase (Ansari and Pandis, 1998). Similar increase (1–2 μg m^{-3}, 28%) of surface nitrate concentrations within the region has been reported by Liu et al. (2018) for the period using a regional chemical transport model. Such a relationship between SO_2 emissions and nitrate concentrations in China has been also pointed out by Leung et al. (2020). In addition, the annual mean concentrations of particulate ammonium and organic aerosols (OA) in East China are reduced by 0.41 μg m^{-3} and 0.13 μg m^{-3}, respectively.

The simulations also reveal that the reductions in sulfate and BC burdens would dampen new particle formation and the growth of particles via condensation and coagulation processes to serve as CCN. Figure 3 shows the longitude-height (pressure in hPa) distribution of the changes (%) in particle number concentrations with the diameters larger than 10 nm (N10) and diagnostic CCN numbers at supersaturation of 0.4% (CCN0.4) along the latitude 35 °N, which is characterized with notable reductions in sulfate and BC burdens. The N10 shows decreases of about 20% in East China (100−130 °E) from the surface to 300 hPa. The simulated CCN0.4 concentrations decrease not only in East China (30%) but also in the middle troposphere (700−200 hPa) over the north Pacific region (10%). According to the sensitivity experiment Exp16SO2, these variations in N10 and CCN0.4 are primarily caused by decreases of particulate sulfate in East China and the downwind regions. The decreases of CCN concentrations would alter the cloud properties through their activation into cloud droplets and subsequently change the radiation budget, which is discussed in the next sections.

3.2 Variations in aerosol optical properties

The pronounced variations of sulfate and BC concentrations between 2008 and 2016 would induce the change in aerosol optical properties, i.e., aerosol optical depth (AOD) and aerosol absorption optical depth (AAOD) at 550 nm. The CAM/ATRAS2 model captures the observed hotspots of AOD (> 0.3) over North Africa, East China, the tropical Atlantic Ocean, and West-South Asia by comparing to the MISR and MODIS measurements (Fig. S4 and Fig. S5). The annual mean AOD for East China in the model (0.25) is lower than that from MISR (0.34) and MODIS (0.41) in the year of 2008. The comparison of regional AOD distributions with satellite-observed measurements are similar to previous modeling studies by CAM models (Sockol and Small Griswold, 2017; He et al., 2015). For instance, Sockol and Small Griswold (2017) present

the differences of AOD between the CAM model and MODIS observations of < −0.2 over East China. The model biases found in some continental outflow areas in the tropics and South Hemisphere may be related to inadequate simulations of sea salt aerosols and their optical properties in the marine atmosphere (Bian et al., 2019; Burgos et al., 2020).

Figure 4 presents the differences of simulated AOD and AAOD at 550 nm between 2008 and 2016. Corresponding to the reductions in sulfate and BC mass concentrations, AOD shows percent decreases of 2−10% over most of East China (marked in black box in Fig. 4), with a region average of 5.2%. The AOD induced by sulfate particles decreases by 35% and has a dominant contribution to the AOD variation. Recent studies find a statistically significant decrease of 10−20% for AOD in the same region over the recent decade based on the remote sensing observations from the surface (AERONET) and space (MODIS and MISR (Fig. S4 and S5)) (Li, 2020; Zhang et al., 2017; Zhao et al., 2017). The annual mean AOD retrieved by MISR varied from 0.34 ±0.07 in 2008 to 0.26 ±0.06 in 2016 and shows a significantly decreasing trend during the period (Fig. S6), while the simulated AOD in the CAM5/ATRAS2 model decreases by about 0.02 between the two years. The underestimation of AOD variability may be partially attributable to the inadequate representation of decadal variations in dust aerosol concentrations from both natural and anthropogenic sources. Recent studies have found a considerable decline in dust episodes over East China during 2007–2014 due to decreased maximum wind speeds and control of air pollution (Wang et al., 2018), and the resulting decrease of dust loadings and their light extinction in air would contribute to the decreases of total AOD, but those effects cannot be fully represented in our simulations. Moreover, the parametrization of aerosol hygroscopicity, especially for light-scattering components (sulfate, nitrate, OA, etc.), can influence modeled aerosol extinction coefficients and is an important source of uncertainties in the estimate of AOD in climate models (Burgos et al., 2020; Reddington et al., 2019).

The simulated annual mean AAOD decreases by about 16% (from 0.018 to 0.015) over East China between the emission years of 2008 and 2016 (Fig. 4), with salient decrease up to 30% in the northern part, which is subject to considerable reductions of BC emissions and resultant column burdens (Fig. 2). We compare the model results with the averaged observations in two AERONET stations (located in the same model horizontal grid and marked in Fig. 4) with long-term records available. The AAOD from AERONET are calculated using the observed AOD and SSA at 550 nm wavelength. The annual mean AOD and AAOD at the AERONET site decrease by about 29% and 40%, respectively, while our model underestimates the variability of AOD, but agrees with observed AAOD variation. Overall, both the simulations and observations demonstrate a clear decline in AOD and AAOD over China between 2008 and 2016 and the reductions in sulfate and BC particles play a critical role in the phenomenon. The resulting effects on the solar radiation budget over China and outflow areas are discussed in the next section.

3.3 Radiative forcings by the change in anthropogenic emissions between 2008 and 2016

Here, we focus on the all-sky aerosol RFs at TOA induced by the inter-annual variation in anthropogenic emissions over China between 2008 and 2016, especially for East China. Both the aerosol shortwave DRF (also termed as RFs due to aerosol-radiation interactions) and shortwave + longwave aerosol effects on CRF (including the semi-direct and indirect effects in this

study) are considered. As shown in Fig. 5 and Fig. S7, the decrease of sulfate mass burdens due to the substantial reduction in SO_2 emissions induce a positive radiative forcing by diminishing the scattering effects of sulfate aerosols. The mean sulfate DRF is +0.38 W m^{-2} over East China during the study period, with high values of more than 0.6 W m^{-2} in the north part that experiences the most notable reduction in sulfate burdens. As a result of SO_2 emission reductions, nitrate concentrations have increased and the merged nitrate and ammonium DRF is estimated to be −0.21 W m^{-2}, though the decrease of particulate ammonium concentrations should yield a positive RF.

The reduction in BC emissions would diminish the absorption effect of BC particles with the decline of the annual mean BC mass burden of 22% over East China between 2008 and 2016 (Fig. 5b and Fig. S8). The resultant BC DRF in the Exp16 case is −0.34 W m^{-2} in the region, accounting for 19% of the BC DRE in 2008. This is 17% higher than the estimate of BC DRF derived from the simulation scenario with BC emission change only (Exp16BC), because the concurrent declines in sulfate concentrations and associated water uptake weaken the absorption enhancement of BC-containing particles, and thus further diminish the positive radiative effects of BC. The absorption enhancements by BC coating materials will be overlooked if BC is externally mixed with other aerosols in climate models, which will significantly underestimate the magnitude of the BC DRF for China between 2008 and 2016. Moreover, the treatment of aging processes of BC is another important factor in determining the radiation effects of BC-containing particles. The models with single mixing state for BC-containing particles (without considering the aging processes from fresh BC to thickly-coated BC) could overestimate (underestimate) the BC DRF when BC-containing particles are assumed to be internally mixed (externally mixed) with other components immediately after emissions (Bond et al., 2013; Matsui et al., 2018a).

We find that the total aerosol DRF due to all components is −0.18 W m^{-2} over East China between the emission years of 2008 and 2016, with the dominant sources from the reductions in SO_2 and BC emissions (Fig. 6a). Noticeably, the BC and sulfate DRF (−0.34 vs. +0.38 W m^{-2}) are almost counterbalanced by each other. After considering the negative nitrate DRF (−0.21 W m^{-2}) resulting from the SO_2 emission reduction, the net DRF from SO_2 emissions between 2008 and 2016 is +0.17 W m^{-2}. OA and dust aerosols have the mean DRF of −0.06 and +0.003 W m^{-2} and contribute few to the total aerosol DRF during the study period. A few uncertainties remain in our estimates of aerosol DRF. The model bias in the AOD variability compared to the satellite observations could transform into the uncertainties in aerosol DRF. As mentioned earlier, the model underestimation of AOD variability during the study period might stem from the uncertainties in dust emissions (natural and anthropogenic sources) and aerosol water uptake by hygroscopic components that are not well represented in current climate models (Burgos et al., 2020). Because the AAOD variation is simulated reasonably, the aerosol scattering effects from dust, sulfate, and OA that dominate AOD may be underestimated in our simulations.

We further consider aerosol effects on CRF with the combination of semi- and in-direct effects, following Ghan (2013). The variation of BC and SO_2 emissions have distinct impacts on cloud radiative effects. First, as mentioned in Section 3.1, the responses of CCN numbers are negligible to the reduction in BC emissions, but of significance to the reduction in SO_2

emissions with a decrease of 20% for the CCN number concentrations at 0.4% supersaturation. The changes in SO_2 emissions and associated decline in sulfate would alter in-direct effects by serving as CCN due to its high hygroscopicity (Twomey, 1974; Andreae and Rosenfeld, 2008). By separating the contribution between SO_2 and BC emissions to CRF (the Exp16SO2 and Exp16BC cases), we find that the annual mean CRF is +0.16 W m^{-2} due to the decreased SO_2 emissions in East China between 2008 and 2016, whilst only −0.05 W m^{-2} due to decreased BC emissions. The positive CRF can be explained by the decrease of simulated CCN numbers (Fig. 3), and it is indicative of less solar radiation outgoing back to the space by clouds and therefore potentially warming the atmosphere. By accounting for the interaction between sulfate and BC particles, we find a net aerosol-induced CRF of +0.13 W m^{-2}, and the total RF that combines aerosol DRF and CRF together is −0.04 W m^{-2} over East China during our study period (Exp08 - Exp16).

While the impacts of SO_2 and BC reductions on RFs (DRF + CRF) are very small locally (−0.04 W m^{-2}), there are markedly positive cloud radiative effects mostly within 0.3−0.6 W m^{-2} in the north Pacific region (Fig. 5), with the mean CRF over the north Pacific (marked in Fig. 5f) of +0.16 W m^{-2}, which are associated with the decrease of CCN due to reductions in SO_2 emissions in China (Fig. S7). Since the aerosol DRF in the north Pacific region is negligible, the aerosol effects on clouds dominate the total radiative forcings when the anthropogenic emissions in China varied from 2008 to 2016. Our results suggest an important role of SO_2 emissions in China in altering the cloud optical properties in the north Pacific. It should be noted that aerosol effects on cloud radiative properties remain the largest uncertainties in calculating global and regional radiation perturbation by anthropogenic aerosols in current climate models, which should be further constrained by measurements of aerosol-cloud interactions.

Furthermore, the inter-annual variations in scattering and absorbing aerosols during 2008–2016 lead to changes in downward radiation flux onto the Earth's surface (Fig. 6). Evident enhancement in surface radiation flux (i.e., surface brightening) take place in East China. The decreases of BC absorption and sulfate scattering effects allow more solar radiation reaching the surface with the temporal changes estimated of +0.96 W m^{-2} $decade^{-1}$ and +0.75 W m^{-2} $decade^{-1}$, respectively (Fig. 6b, c). Increases of nitrate and OA concentrations diminish the downward surface solar shortwave radiation. The net change in the annul-mean surface radiation due to all aerosols is as large as 1.1 W m^{-2} $decade^{-1}$ (Fig. 6a). Compared to those induced by aerosols-radiation interactions, the aerosol-induced cloud effects on surface radiation are minor (+0.20 W m^{-2} $decade^{-1}$). With the consideration of the overall effects by the differences in emissions between 2008 and 2016, the simulated downward radiation fluxes onto surface increase by +1.3 W m^{-2} $decade^{-1}$. Our result is close to the long-term observational trend of the shortwave energy balance in China from 2000–2015 provided by Schwarz et al. (2020). They have shown a positive trend in downward surface shortwave radiation of +1.4 ±0.2 W m^{-2} $decade^{-1}$ for the period, which is considered to be mainly driven by the reductions in the atmospheric shortwave absorption. The decadal change in solar absorption of BC is estimated to be −1.4 W m^{-2} $decade^{-1}$ in our simulations, 56% lower than the observed total atmospheric shortwave absorption (−3.2 ±0.4 W m^{-2} $decade^{-1}$) based on observational data for the similar period (Schwarz et al., 2020). Apart from BC, other absorbing aerosol components, like anthropogenic magnetite (Matsui et al., 2018b) and brown carbon from fossil fuels and biomass or biofuel

burning sources (Zhang et al., 2020; Yan et al., 2017) may also contribute to decadal variation of atmospheric shortwave absorption in China. In summary, our simulation results provide the first modeling evidence for that the mitigation of aerosol pollution, particularly of BC and sulfate, critically determines the surface brightening observed in China over the recent decade (Yang et al., 2019; Schwarz et al., 2020).

In order to understand how aerosol DRF and CRF respond to future emissions, we refer to the projected anthropogenic emission scenarios in China recently developed by Tong et al. (2020) for 2030 and 2050. For these scenarios, they have integrated the shared socio-economic pathways (SSPs), climate targets of Representative Concentration Pathways (RCPs), and local air pollution control measures to create dynamic projection of China's emissions in the future decades. Here, among their designed scenarios, we choose the SSP1-RCP26-BHE (Best Health Effect), which denotes the best-available environmental policies and therefore the largest reductions of emissions, to predict the upper bound of climate effects from anthropogenic aerosols. We performed the simulations by using the same meteorological nudging with the historical case for 2008 (Exp08) and scaling anthropogenic emissions in China separately from 2016 to 2030 and from 2016 to 2050 following Tong et al. (2020) (Table S3). The projected emissions of greenhouse gases are not considered and only the aerosol effects on radiation budget are shown here. We find that under the strictest air pollution control policies, the aerosol DRF estimates are +0.24 W m^{-2} between 2016−2030 and +0.64 W m^{-2} between 2016−2050 over East China (Fig. 7). The total RFs with the combination of DRF and CRF reach +0.55 W m^{-2} and +1.23 W m^{-2}, respectively. For this scenario, although BC emissions keep decreasing in the future, the reductions in scattering aerosols like OA and nitrate induce high positive RFs. The DRF of OA and nitrate due to aerosol-radiation interactions are +0.27 and +0.52 W m^{-2} between 2016−2050. Similar to our case, Samset et al. (2019) have estimated a net radiative forcing induced by sulfate and BC aerosols of approximately +0.5 W m^{-2} over China under a strong air-quality policy (SSP1-1.9) from 2014–2030 using the climate model Oslo CTM3 with an oversimplification of aerosol-cloud interaction effects. In addition, the aerosol effect on cloud forcings in north Pacific is around +0.2 W m^{-2} for the both 2016−2030 and 2016−2050 cases and lower than the CRF estimate in East China.

This study mainly focuses on the impacts of emission variations on aerosol radiative forcings, while the meteorological conditions could also affect aerosol forcings. We perform another simulation experiment with the meteorological nudging and anthropogenic emissions both for 2016 (referred to as Exp16m) and compared the resulting aerosol DRF with those found in the Exp16 case (only emission variation included; see Table S4). Note that in the Exp16m case, the aerosol effects on cloud forcings cannot be separated from the variation in meteorological fields in the model. The changes in BC and sulfate mass burdens for Exp08-Exp16m (differences between the Exp08 and Exp16m cases) are close to those for Exp08-Exp16, but the BC DRF is reduced by about 29% due to variation in meteorology during 2008–2016. Nevertheless, both our results and previous studies (Liu et al., 2020; Zhang et al., 2019) demonstrate that the decadal variations in aerosol pollutions and DRF are dominated by the reductions in anthropogenic emissions over the past decade.

4. Summary

In this study, we quantify the all-sky aerosol RFs for China (especially East China) due to the substantial variations of anthropogenic emissions in the country between 2008 and 2016 using a global climate model. Our simulations demonstrate that the dramatic reductions (−57%) in SO_2 emissions decrease sulfate mass burdens by 35% in East China and 18% in north Pacific, while the burdens of BC are reduced by 22% due to decreased BC emissions (−27%) for this period. It is estimated that the reductions in SO_2 emissions give rise to +0.38 W m^{-2} for sulfate DRF at TOA, −0.21 W m^{-2} for nitrate and ammonium combined DRF, and +0.13 W m^{-2} for aerosol-induced CRF, and meanwhile the BC emission reduction induce a cooling effect of −0.34 W m^{-2} over East China. Since the effects from other aerosol components are negligible in our simulations, the changes in SO_2 and BC emissions dominate the aerosol RFs between 2008 and 2016. Their net RF is −0.04 W m^{-2} over East China, implying a counterbalancing effect. It's also interesting to note that the declines in sulfate concentrations and associated water uptake weaken the absorption enhancement of BC-containing particles, and contribute to 17% of the BC DRF compared to that with BC emission changed only. Such an effect cannot be detected without an explicit treatment of absorption enhancement for internally mixed BC particles, as developed in our model (Matsui, 2020).

Moreover, in agreement with the observational-based study on the long-term trend of the downward shortwave radiation that reaches the Earth's surface (Schwarz et al., 2020), our simulations indicate the surface brightening over China from 2008 to 2016. It is estimated that the annul mean downward solar radiation flux at surface shows a clear enhancement of +1.3 W m^{-2} $decade^{-1}$ because of the diminishment of BC absorption and sulfate scattering effects in the atmosphere. The results provide the direct modeling evidence for the cause of observed surface brightening in China over the recent decade. Even though the BC and SO_2 emissions exert an overall balanced radiative effect at TOA, the solar radiation budgets have been perturbed both at surface and within the atmosphere, which would influence the surface temperature, boundary layer development, and East Asia monsoon (Huang et al., 2018; Hong et al., 2020; Li et al., 2016b).

While the radiative forcing at TOA is small locally due to the counteracted effects of SO_2 and BC emissions, there is relatively large positive change of about +0.16 W m^{-2} due to aerosol effects on clouds in the north Pacific remote region, primarily caused by reductions in sulfate particles and their effects on cloud properties via CCN activation. The decrease of sulfate burdens (−18%) in the north Pacific due to the emission control of SO_2 in China results in more than 10% decreases of CCN0.4 in the middle troposphere (700−200 hPa) over the north Pacific, which would reduce the cloud droplet numbers and weaken the cloud albedo. Therefore, our results highlight the importance of China's SO_2 emissions not only in the contribution to the local radiative forcing, but also in altering the radiation budget in the downwind Pacific regions through the transport of secondary sulfate aerosols and associated effects on clouds.

We further predict the aerosol radiative effects using the recently developed China's emission scenario for 2030 and 2050. The results demonstrate that under the strictest environmental policies for China, the total aerosol RFs (DRF + CRF) from the projected emission scenarios are +0.55 W m^{-2} between 2016−2030 and +1.23 W m^{-2} between 2016−2050. These effects should

be considered by combining with the emission projection of greenhouse gases to better evaluate the responses of climate to future human emissions over the regional and global scales.

Appendix A: List of acronyms

AERONET	Aerosol robotic network
AOD	Aerosol optical depth
AAOD	Absorption aerosol optical depth
ATRAS2	Aerosol two-dimensional bin module for formation and aging simulation version 2
BC	Black carbon
BHE	Best health effect
CAM5	Community Atmospheric Model version 5
CCN	Cloud condensation nuclei
CCN0.4	CCN number concentrations at supersaturation of 0.4%
CRF	Cloud radiative forcing
DRE	Direct radiative effect
DRF	Direct radiative forcing
EANET	Acid deposition monitoring network in East Asia
HIPPO	HIAPER Pole-to-Pole Observations
IPCC AR5	The Fifth assessment report of the Intergovernmental Panel on Climate Change
MEIC	Multi-resolution emission inventory for China
MERRA2	Modern-Era retrospective analysis for research and applications version 2
MISR	Multi-angle imaging spectroradiometer
MODIS	Moderate Resolution Imaging Spectroradiometer
MOZART	Model for ozone and related chemical tracers
N10	particle number concentrations with the diameter larger than 10 nm
NOx	Nitrogen oxides
OC	Organic carbon
OA	Organic aerosol
OMI	Ozone Monitoring Instrument
RCP	Representative Concentration Pathways
RF	Radiative forcing
RFari	Radiative forcing due to aerosol-radiation interaction
SO_2	Sulfur dioxide
SSA	Single scatter albedo

SSP	Shared socio-economic pathways
TOA	Top of the atmosphere

Data availability. EANET observation data is freely available from the online website (https://monitoring.eanet.asia/document/public/index, last access: 10 March 2020). AERONET data for AOD and SSA can be accessed from Goddard Space Flight Center (https://aeronet.gsfc.nasa.gov/new_web/data.html, last access: 20 April 2020). MISR Level-3 data are available from the Atmospheric Science Data Center at NASA (https://l0dup05.larc.nasa.gov/, last access: 6 October 2020). Monthly MODIS AOD data are provided by NASA Earth Observations (NEO) (https://neo.sci.gsfc.nasa.gov/view.php?datasetId=MODAL2_M_AER_OD, last access: 9 September 2020). HIPPO observations of BC vertical profiles are taken from the Earth Observing Laboratory (EOL) HIPPO data archive (http://www.eol.ucar.edu/projects/hippo/, last access: 10 October 2020). OMI SO_2 columns are taken from NASA AVDC (https://avdc.gsfc.nasa.gov/pub/, last access: 16 October 2020). Historical and future anthropogenic emissions for China are provided from the MEIC database (http://www.meicmodel.org/, last access: 15 May 2020).

Author contribution. ML and HM designed the study and wrote the paper. ML performed the simulations and analyzed the results.

Competing interests. The authors declare that they have no conflict of interest.

Acknowledgements. This work was supported by the Ministry of Education, Culture, Sports, Science, and Technology and the Japan Society for the Promotion of Science (MEXT/JSPS) KAKENHI Grant Numbers JP17H04709, JP16H01770, JP19H04253, JP19H05699, and JP19KK0265 and by the MEXT Arctic Challenge for Sustainability (ArCS, Program Grant Number JPMXD1300000000) and ArCS-II projects. This work was also supported by the Environment Research and Technology Development Fund (2–1703 and 2-2003) of the Environmental Restoration and Conservation Agency.

References

Andreae, M. O., and Rosenfeld, D.: Aerosol–cloud–precipitation interactions. Part 1. The nature and sources of cloud-active aerosols, Earth Sci. Rev., 89, 13-41, https://doi.org/10.1016/j.earscirev.2008.03.001, 2008.

Ansari, A. S., and Pandis, S. N.: Response of Inorganic PM to Precursor Concentrations, Environ. Sci. Technol., 32, 2706-2714, 10.1021/es971130j, 1998.

Bian, H., Froyd, K., Murphy, D. M., Dibb, J., Darmenov, A., Chin, M., Colarco, P. R., da Silva, A., Kucsera, T. L., Schill, G., Yu, H., Bui, P., Dollner, M., Weinzierl, B., and Smirnov, A.: Observationally constrained analysis of sea salt aerosol in the marine atmosphere, Atmos. Chem. Phys., 19, 10773-10785, 10.5194/acp-19-10773-2019, 2019.

Bond, T. C., Doherty, S. J., Fahey, D. W., Forster, P. M., Berntsen, T., DeAngelo, B. J., Flanner, M. G., Ghan, S., Kärcher, B., Koch, D., Kinne, S., Kondo, Y., Quinn, P. K., Sarofim, M. C., Schultz, M. G., Schulz, M., Venkataraman, C., Zhang, H., Zhang, S., Bellouin, N., Guttikunda, S. K., Hopke, P. K., Jacobson, M. Z., Kaiser, J. W., Klimont, Z., Lohmann, U.,

Schwarz, J. P., Shindell, D., Storelvmo, T., Warren, S. G., and Zender, C. S.: Bounding the role of black carbon in the climate system: A scientific assessment, J. Geophys. Res.-Atmos, 118, 5380-5552, 10.1002/jgrd.50171, 2013.

Boucher, O., Randall, D., Artaxo, P., Bretherton, C., Feingold, G., Forster, P., Kerminen, V.-M., Kondo, Y., and Liao, H.: Clouds and aerosols. In T. F. Stocker, et al. (Eds.), Climate change 2013: The physical science basis, contribution of Working Group I to the Fifth Assessment Report of the Intergovernmental Panel on Climate Change (pp. 571–658), Cambridge, United Kingdom and New York: Cambridge University Press, 2013.

Burgos, M. A., Andrews, E., Titos, G., Benedetti, A., Bian, H., Buchard, V., Curci, G., Kipling, Z., Kirkevåg, A., Kokkola, H., Laakso, A., Letertre-Danczak, J., Lund, M. T., Matsui, H., Myhre, G., Randles, C., Schulz, M., van Noije, T., Zhang, K., Alados-Arboledas, L., Baltensperger, U., Jefferson, A., Sherman, J., Sun, J., Weingartner, E., and Zieger, P.: A global model–measurement evaluation of particle light scattering coefficients at elevated relative humidity, Atmos. Chem. Phys., 20, 10231-10258, 10.5194/acp-20-10231-2020, 2020.

Charlson, R. J., Schwartz, S. E., Hales, J. M., Cess, R. D., Coakley, J. A., Hansen, J. E., and Hofmann, D. J.: Climate Forcing by Anthropogenic Aerosols, Science, 255, 423, 10.1126/science.255.5043.423, 1992.

Cheng, Y., Zheng, G., Wei, C., Mu, Q., Zheng, B., Wang, Z., Gao, M., Zhang, Q., He, K., Carmichael, G., Pöschl, U., and Su, H.: Reactive nitrogen chemistry in aerosol water as a source of sulfate during haze events in China, Sci. Adv., 2, e1601530, 10.1126/sciadv.1601530, 2016.

Chung, S. H., and Seinfeld, J. H.: Global distribution and climate forcing of carbonaceous aerosols, J. Geophys. Res.-Atmos, 107, AAC 14-11-AAC 14-33, 10.1029/2001JD001397, 2002.

Garay, M. J., Witek, M. L., Kahn, R. A., Seidel, F. C., Limbacher, J. A., Bull, M. A., Diner, D. J., Hansen, E. G., Kalashnikova, O. V., Lee, H., Nastan, A. M., and Yu, Y.: Introducing the 4.4 km spatial resolution Multi-Angle Imaging SpectroRadiometer (MISR) aerosol product, Atmos. Meas. Tech., 13, 593-628, 10.5194/amt-13-593-2020, 2020.

Ghan, S. J.: Technical Note: Estimating aerosol effects on cloud radiative forcing, Atmos. Chem. Phys., 13, 9971-9974, 10.5194/acp-13-9971-2013, 2013.

He, J., Zhang, Y., Glotfelty, T., He, R., Bennartz, R., Rausch, J., and Sartelet, K.: Decadal simulation and comprehensive evaluation of CESM/CAM5.1 with advanced chemistry, aerosol microphysics, and aerosol-cloud interactions, J. Adv. Model. Earth Syst., 7, 110-141, 10.1002/2014ms000360, 2015.

Hoesly, R. M., Smith, S. J., Feng, L., Klimont, Z., Janssens-Maenhout, G., Pitkanen, T., Seibert, J. J., Vu, L., Andres, R. J., Bolt, R. M., Bond, T. C., Dawidowski, L., Kholod, N., Kurokawa, J. I., Li, M., Liu, L., Lu, Z., Moura, M. C. P., O'Rourke, P. R., and Zhang, Q.: Historical (1750–2014) anthropogenic emissions of reactive gases and aerosols from the Community Emissions Data System (CEDS), Geosci. Model Dev., 11, 369-408, 10.5194/gmd-11-369-2018, 2018.

Hong, C., Zhang, Q., Zhang, Y., Davis, S. J., Zhang, X., Tong, D., Guan, D., Liu, Z., and He, K.: Weakening aerosol direct radiative effects mitigate climate penalty on Chinese air quality, Nat. Clim. Change, 10, 845-850, 10.1038/s41558-020-0840-y, 2020.

Huang, X., Song, Y., Zhao, C., Li, M., Zhu, T., Zhang, Q., and Zhang, X.: Pathways of sulfate enhancement by natural and anthropogenic mineral aerosols in China, J. Geophys. Res.-Atmos, 119, 14,165-114,179, 10.1002/2014JD022301, 2014.

Huang, X., Song, Y., Zhao, C., Cai, X., Zhang, H., and Zhu, T.: Direct Radiative Effect by Multicomponent Aerosol over China, J. Clim., 28, 3472-3495, 10.1175/jcli-d-14-00365.1, 2015.

Huang, X., Wang, Z., and Ding, A.: Impact of Aerosol-PBL Interaction on Haze Pollution: Multiyear Observational Evidences in North China, Geophys. Res. Lett., 45, 8596-8603, 10.1029/2018gl079239, 2018.

Hung, H.-M., and Hoffmann, M. R.: Oxidation of Gas-Phase SO2 on the Surfaces of Acidic Microdroplets: Implications for Sulfate and Sulfate Radical Anion Formation in the Atmospheric Liquid Phase, Environ. Sci. Technol., 49, 13768-13776, 10.1021/acs.est.5b01658, 2015.

Itahashi, S., Yumimoto, K., Uno, I., Hayami, H., Fujita, S. I., Pan, Y., and Wang, Y.: A 15-year record (2001–2015) of the ratio of nitrate to non-sea-salt sulfate in precipitation over East Asia, Atmos. Chem. Phys., 18, 2835-2852, 10.5194/acp-18-2835-2018, 2018.

Jacobson, M. Z.: Strong radiative heating due to the mixing state of black carbon in atmospheric aerosols, Nature, 409, 695-697, 10.1038/35055518, 2001.

Kanaya, Y., Yamaji, K., Miyakawa, T., Taketani, F., Zhu, C., Choi, Y., Komazaki, Y., Ikeda, K., Kondo, Y., and Klimont, Z.: Rapid reduction in black carbon emissions from China: evidence from 2009–2019 observations on Fukue Island, Japan, Atmos. Chem. Phys., 20, 6339-6356, 10.5194/acp-20-6339-2020, 2020.

Koch, D., and Del Genio, A. D.: Black carbon semi-direct effects on cloud cover: review and synthesis, Atmos. Chem. Phys., 10, 7685-7696, 10.5194/acp-10-7685-2010, 2010.

Kulkarni, G., China, S., Liu, S., Nandasiri, M., Sharma, N., Wilson, J., Aiken, A. C., Chand, D., Laskin, A., Mazzoleni, C., Pekour, M., Shilling, J., Shutthanandan, V., Zelenyuk, A., and Zaveri, R. A.: Ice nucleation activity of diesel soot particles at cirrus relevant temperature conditions: Effects of hydration, secondary organics coating, soot morphology, and coagulation, Geophys. Res. Lett., 43, 3580-3588, 10.1002/2016GL068707, 2016.

Leung, D. M., Shi, H., Zhao, B., Wang, J., Ding, E. M., Gu, Y., Zheng, H., Chen, G., Liou, K. N., Wang, S., Fast, J. D., Zheng, G., Jiang, J., Li, X., and Jiang, J. H.: Wintertime Particulate Matter Decrease Buffered by Unfavorable Chemical Processes Despite Emissions Reductions in China, Geophys. Res. Lett., 47, 10.1029/2020gl087721, 2020.

Li, B., Gasser, T., Ciais, P., Piao, S., Tao, S., Balkanski, Y., Hauglustaine, D., Boisier, J. P., Chen, Z., Huang, M., Li, L. Z., Li, Y., Liu, H., Liu, J., Peng, S., Shen, Z., Sun, Z., Wang, R., Wang, T., Yin, G., Yin, Y., Zeng, H., Zeng, Z., and Zhou, F.: The contribution of China's emissions to global climate forcing, Nature, 531, 357-361, 10.1038/nature17165, 2016a.

Li, C., McLinden, C., Fioletov, V., Krotkov, N., Carn, S., Joiner, J., Streets, D., He, H., Ren, X., Li, Z., and Dickerson, R. R.: India Is Overtaking China as the World's Largest Emitter of Anthropogenic Sulfur Dioxide, Sci Rep, 7, 14304, 10.1038/s41598-017-14639-8, 2017.

Li, J.: Pollution Trends in China from 2000 to 2017: A Multi-Sensor View from Space, Remote Sensing, 12, 10.3390/rs12020208, 2020.

Li, Z., Lau, W. K. M., Ramanathan, V., Wu, G., Ding, Y., Manoj, M. G., Liu, J., Qian, Y., Li, J., Zhou, T., Fan, J., Rosenfeld, D., Ming, Y., Wang, Y., Huang, J., Wang, B., Xu, X., Lee, S. S., Cribb, M., Zhang, F., Yang, X., Zhao, C., Takemura, T., Wang, K., Xia, X., Yin, Y., Zhang, H., Guo, J., Zhai, P. M., Sugimoto, N., Babu, S. S., and Brasseur, G. P.: Aerosol and monsoon climate interactions over Asia, Rev. Geophys., 54, 866-929, 10.1002/2015RG000500, 2016b.

Liu, M., Huang, X., Song, Y., Xu, T., Wang, S., Wu, Z., Hu, M., Zhang, L., Zhang, Q., Pan, Y., Liu, X., and Zhu, T.: Rapid SO2 emission reductions significantly increase tropospheric ammonia concentrations over the North China Plain, Atmos. Chem. Phys., 18, 17933-17943, 10.5194/acp-18-17933-2018, 2018.

Liu, M., Song, Y., Xu, T., Xu, Z., Wang, T., Yin, L., Jia, X., and Tang, J.: Trends of Precipitation Acidification and Determining Factors in China During 2006–2015, J. Geophys. Res.-Atmos, 125, e2019JD031301, 10.1029/2019JD031301, 2020.

Liu, X., Easter, R. C., Ghan, S. J., Zaveri, R., Rasch, P., Shi, X., Lamarque, J. F., Gettelman, A., Morrison, H., Vitt, F., Conley, A., Park, S., Neale, R., Hannay, C., Ekman, A. M. L., Hess, P., Mahowald, N., Collins, W., Iacono, M. J., Bretherton, C. S., Flanner, M. G., and Mitchell, D.: Toward a minimal representation of aerosols in climate models: description and evaluation in the Community Atmosphere Model CAM5, Geosci. Model Dev., 5, 709-739, 10.5194/gmd-5-709-2012, 2012.

Matsui, H., Koike, M., Kondo, Y., Fast, J. D., and Takigawa, M.: Development of an aerosol microphysical module: Aerosol Two-dimensional bin module for foRmation and Aging Simulation (ATRAS), Atmos. Chem. Phys., 14, 10315-10331, 10.5194/acp-14-10315-2014, 2014.

Matsui, H.: Black carbon simulations using a size- and mixing-state-resolved three-dimensional model: 2. Aging timescale and its impact over East Asia, J. Geophys. Res.-Atmos, 121, 1808–1821, 10.1002/2015JD023999, 2016.

Matsui, H.: Development of a global aerosol model using a two-dimensional sectional method: 1. Model design, J. Adv. Model. Earth Syst., 9, 1921-1947, 10.1002/2017ms000936, 2017.

Matsui, H., and Mahowald, N.: Development of a global aerosol model using a two-dimensional sectional method: 2. Evaluation and sensitivity simulations, J. Adv. Model. Earth Syst., 9, 1887-1920, 10.1002/2017ms000937, 2017.

Matsui, H., Hamilton, D. S., and Mahowald, N. M.: Black carbon radiative effects highly sensitive to emitted particle size when resolving mixing-state diversity, Nat Commun, 9, 3446, 10.1038/s41467-018-05635-1, 2018a.

Matsui, H., Mahowald, N. M., Moteki, N., Hamilton, D. S., Ohata, S., Yoshida, A., Koike, M., Scanza, R. A., and Flanner, M. G.: Anthropogenic combustion iron as a complex climate forcer, Nat Commun, 9, 1593, 10.1038/s41467-018-03997-0, 2018b.

Matsui, H.: Black carbon absorption efficiency under preindustrial and present-day conditions simulated by a size- and mixing-state-resolved global aerosol model, J. Geophys. Res.-Atmos, 125, e2019JD032316, 10.1029/2019JD032316, 2020.

Morrison, H., and Gettelman, A.: A New Two-Moment Bulk Stratiform Cloud Microphysics Scheme in the Community Atmosphere Model, Version 3 (CAM3). Part I: Description and Numerical Tests, J. Clim., 21, 3642-3659, 10.1175/2008jcli2105.1, 2008.

Myhre, G., Samset, B. H., Schulz, M., Balkanski, Y., Bauer, S., Berntsen, T. K., Bian, H., Bellouin, N., Chin, M., Diehl, T., Easter, R. C., Feichter, J., Ghan, S. J., Hauglustaine, D., Iversen, T., Kinne, S., Kirkevåg, A., Lamarque, J. F., Lin, G., Liu, X., Lund, M. T., Luo, G., Ma, X., van Noije, T., Penner, J. E., Rasch, P. J., Ruiz, A., Seland, Ø., Skeie, R. B., Stier, P., Takemura, T., Tsigaridis, K., Wang, P., Wang, Z., Xu, L., Yu, H., Yu, F., Yoon, J. H., Zhang, K., Zhang, H., and Zhou, C.: Radiative forcing of the direct aerosol effect from AeroCom Phase II simulations, Atmos. Chem. Phys., 13, 1853-1877, 10.5194/acp-13-1853-2013, 2013.

Paulot, F., Paynter, D., Ginoux, P., Naik, V., and Horowitz, L. W.: Changes in the aerosol direct radiative forcing from 2001 to 2015: observational constraints and regional mechanisms, Atmos. Chem. Phys., 18, 13265-13281, 10.5194/acp-18-13265-2018, 2018.

Reddington, C. L., Morgan, W. T., Darbyshire, E., Brito, J., Coe, H., Artaxo, P., Scott, C. E., Marsham, J., and Spracklen, D. V.: Biomass burning aerosol over the Amazon: analysis of aircraft, surface and satellite observations using a global aerosol model, Atmos. Chem. Phys., 19, 9125-9152, 10.5194/acp-19-9125-2019, 2019.

Samset, B. H., Lund, M. T., Bollasina, M., Myhre, G., and Wilcox, L.: Emerging Asian aerosol patterns, Nat. Geosci., 12, 582-584, 10.1038/s41561-019-0424-5, 2019.

Sayer, A. M., Munchak, L. A., Hsu, N. C., Levy, R. C., Bettenhausen, C., and Jeong, M. J.: MODIS Collection 6 aerosol products: Comparison between Aqua's e-Deep Blue, Dark Target, and "merged" data sets, and usage recommendations, J. Geophys. Res.-Atmos, 119, 13,965-913,989, 10.1002/2014JD022453, 2014.

Schwarz, J. P., Samset, B. H., Perring, A. E., Spackman, J. R., Gao, R. S., Stier, P., Schulz, M., Moore, F. L., Ray, E. A., and Fahey, D. W.: Global-scale seasonally resolved black carbon vertical profiles over the Pacific, Geophys Res Lett, 40, 5542-5547, 10.1002/2013GL057775, 2013.

Schwarz, M., Folini, D., Yang, S., Allan, R. P., and Wild, M.: Changes in atmospheric shortwave absorption as important driver of dimming and brightening, Nat. Geosci., 13, 110-115, 10.1038/s41561-019-0528-y, 2020.

Seinfeld, J. H., and Pandis, S. N.: Atmospheric Chemistry and Physics: From Air Pollution to Climate Change, Third edition ed., John Wiley & Sons, Inc., 2016.

Sockol, A., and Small Griswold, J. D.: Intercomparison between CMIP5 model and MODIS satellite-retrieved data of aerosol optical depth, cloud fraction, and cloud-aerosol interactions, Earth Space Sci., 4, 485-505, 10.1002/2017ea000288, 2017.

Stier, P., Seinfeld, J. H., Kinne, S., Feichter, J., and Boucher, O.: Impact of nonabsorbing anthropogenic aerosols on clear-sky atmospheric absorption, J. Geophys. Res.-Atmos, 111, 10.1029/2006JD007147, 2006.

Tong, D., Cheng, J., Liu, Y., Yu, S., Yan, L., Hong, C., Qin, Y., Zhao, H., Zheng, Y., Geng, G., Li, M., Liu, F., Zhang, Y., Zheng, B., Clarke, L., and Zhang, Q.: Dynamic projection of anthropogenic emissions in China: methodology and 2015-2050 emission pathways under a range of socio-economic, climate policy, and pollution control scenarios, Atmos. Chem. Phys., 20, 5729-5757, 10.5194/acp-20-5729-2020, 2020.

Twomey, S.: Pollution and the planetary albedo, Atmospheric Environment (1967), 8, 1251-1256, https://doi.org/10.1016/0004-6981(74)90004-3, 1974.

Wang, X., Liu, J., Che, H., Ji, F., and Liu, J.: Spatial and temporal evolution of natural and anthropogenic dust events over northern China, Sci Rep, 8, 2141, 10.1038/s41598-018-20382-5, 2018.

Wei, C., Wang, M. H., Fu, Q. Y., Dai, C., Huang, R., and Bao, Q.: Temporal Characteristics and Potential Sources of Black Carbon in Megacity Shanghai, China, J. Geophys. Res.-Atmos, 125, 10.1029/2019jd031827, 2020.

Wofsy, S. C.: HIAPER Pole-to-Pole Observations (HIPPO): fine-grained, global-scale measurements of climatically important atmospheric gases and aerosols, 369, 2073-2086, doi:10.1098/rsta.2010.0313, 2011.

Xia, Y., Wu, Y., Huang, R.-J., Xia, X., Tang, J., Wang, M., Li, J., Wang, C., Zhou, C., and Zhang, R.: Variation in black carbon concentration and aerosol optical properties in Beijing: Role of emission control and meteorological transport variability, Chemosphere, 254, 10.1016/j.chemosphere.2020.126849, 2020.

Yan, C., Zheng, M., Bosch, C., Andersson, A., Desyaterik, Y., Sullivan, A. P., Collett, J. L., Zhao, B., Wang, S., He, K., and Gustafsson, Ö.: Important fossil source contribution to brown carbon in Beijing during winter, Sci. Rep., 7, 43182, 10.1038/srep43182, 2017.

Yang, S., Wang, X. L., and Wild, M.: Causes of Dimming and Brightening in China Inferred from Homogenized Daily Clear-Sky and All-Sky in situ Surface Solar Radiation Records (1958–2016), J. Clim., 32, 5901-5913, 10.1175/jcli-d-18-0666.1, 2019.

Zhang, A., Wang, Y., Zhang, Y., Weber, R. J., Song, Y., Ke, Z., and Zou, Y.: Modeling the global radiative effect of brown carbon: a potentially larger heating source in the tropical free troposphere than black carbon, Atmos. Chem. Phys., 20, 1901-1920, 10.5194/acp-20-1901-2020, 2020.

Zhang, J., Reid, J. S., Alfaro-Contreras, R., and Xian, P.: Has China been exporting less particulate air pollution over the past decade?, Geophys. Res. Lett., 44, 2941-2948, 10.1002/2017gl072617, 2017.

Zhang, Q., Zheng, Y., Tong, D., Shao, M., Wang, S., Zhang, Y., Xu, X., Wang, J., He, H., Liu, W., Ding, Y., Lei, Y., Li, J., Wang, Z., Zhang, X., Wang, Y., Cheng, J., Liu, Y., Shi, Q., Yan, L., Geng, G., Hong, C., Li, M., Liu, F., Zheng, B., Cao, J., Ding, A., Gao, J., Fu, Q., Huo, J., Liu, B., Liu, Z., Yang, F., He, K., and Hao, J.: Drivers of improved PM2.5 air quality in China from 2013 to 2017, Proceedings of the National Academy of Sciences, 116, 24463, 10.1073/pnas.1907956116, 2019.

Zhao, B., Jiang, J. H., Gu, Y., Diner, D., Worden, J., Liou, K.-N., Su, H., Xing, J., Garay, M., and Huang, L.: Decadal-scale trends in regional aerosol particle properties and their linkage to emission changes, Environ. Res. Lett., 12, 10.1088/1748-9326/aa6cb2, 2017.

Zheng, B., Tong, D., Li, M., Liu, F., Hong, C., Geng, G., Li, H., Li, X., Peng, L., Qi, J., Yan, L., Zhang, Y., Zhao, H., Zheng, Y., He, K., and Zhang, Q.: Trends in China's anthropogenic emissions since 2010 as the consequence of clean air actions, Atmos. Chem. Phys., 18, 14095-14111, 10.5194/acp-18-14095-2018, 2018.

Table 1. Model simulation experiments with different emission scenarios for China

	SO_2	BC	Others
Exp08	2008	2008	2008
Exp16	2016	2016	2016
Exp16SO2	2016	2008	2008
Exp16BC	2008	2016	2008

Table 2. Anthropogenic emissions for major species in China and East China (EC) between 2008 and 2016 (units: Tg year^{-1}). The emissions are derived from the MEIC database (Zheng et al., 2018). The geographical range of the EC is shown in Fig. 1

	2008		2016	
	China	EC	China	EC
BC	1.7	1.5	1.3	1.1
NO_x	24	21	23	19
OC	3.2	2.7	2.3	1.9
$PM_{2.5}$	12	11	8.1	6.9
SO_2	30	28	13	12

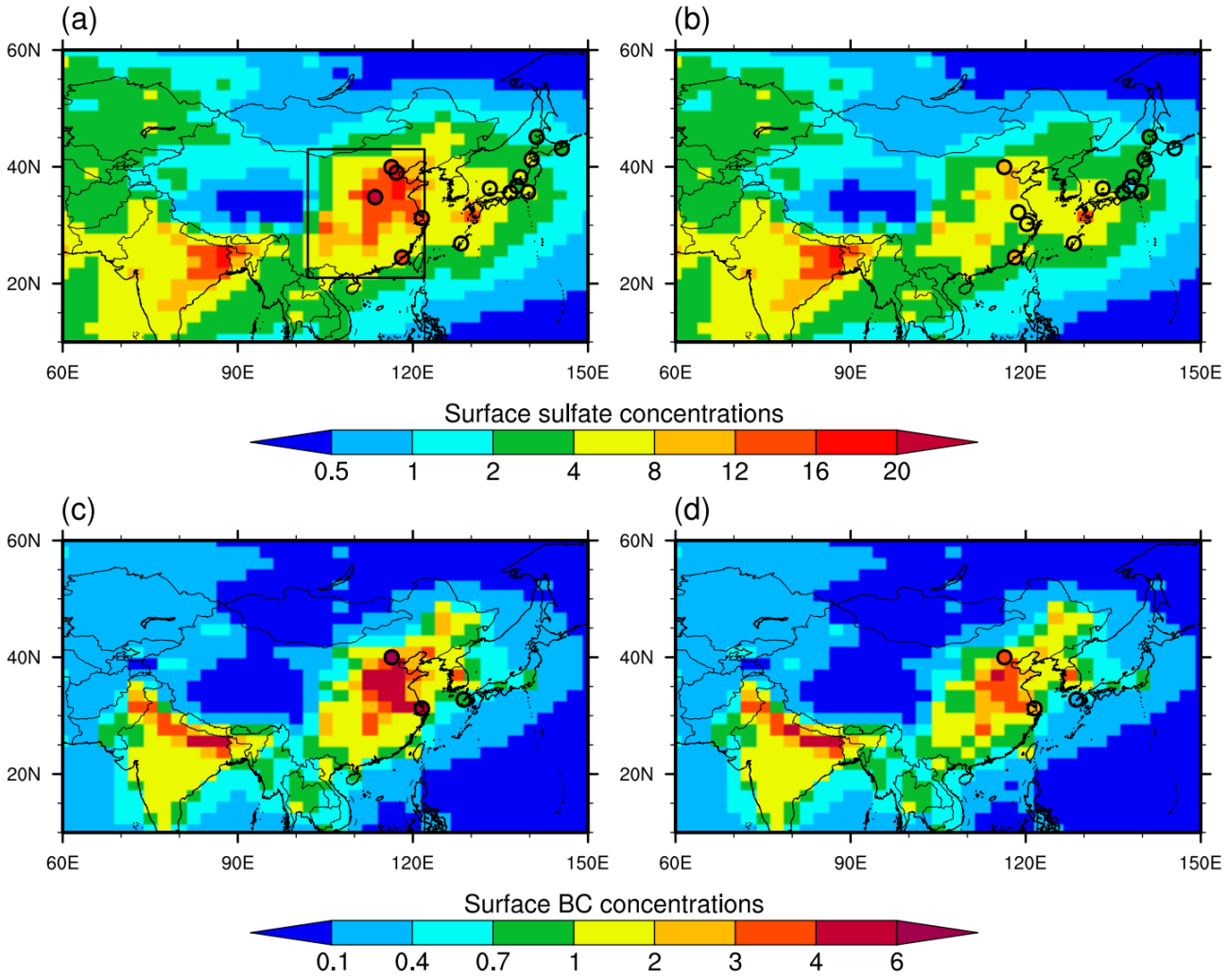

Figure 1. Map of simulated surface $PM_{2.5}$ sulfate (a-b) and BC (c-d) concentrations (units: μg m^{-3}) over China and surrounding areas between 2008 (left column) and 2016 (right column). The observations of the annual mean sulfate and BC concentrations obtained from EANET and literature (Table S1) are shown for comparison. The geographical range of East China (21°−43° N, 102°−122° E) is marked in Fig. 1a. The annual mean surface BC concentrations observed at Fukue island (32.75 ºN, 128.68º E) in western Japan for 2010 (Fig. 1c) and 2016 (Fig. 1d) are marked

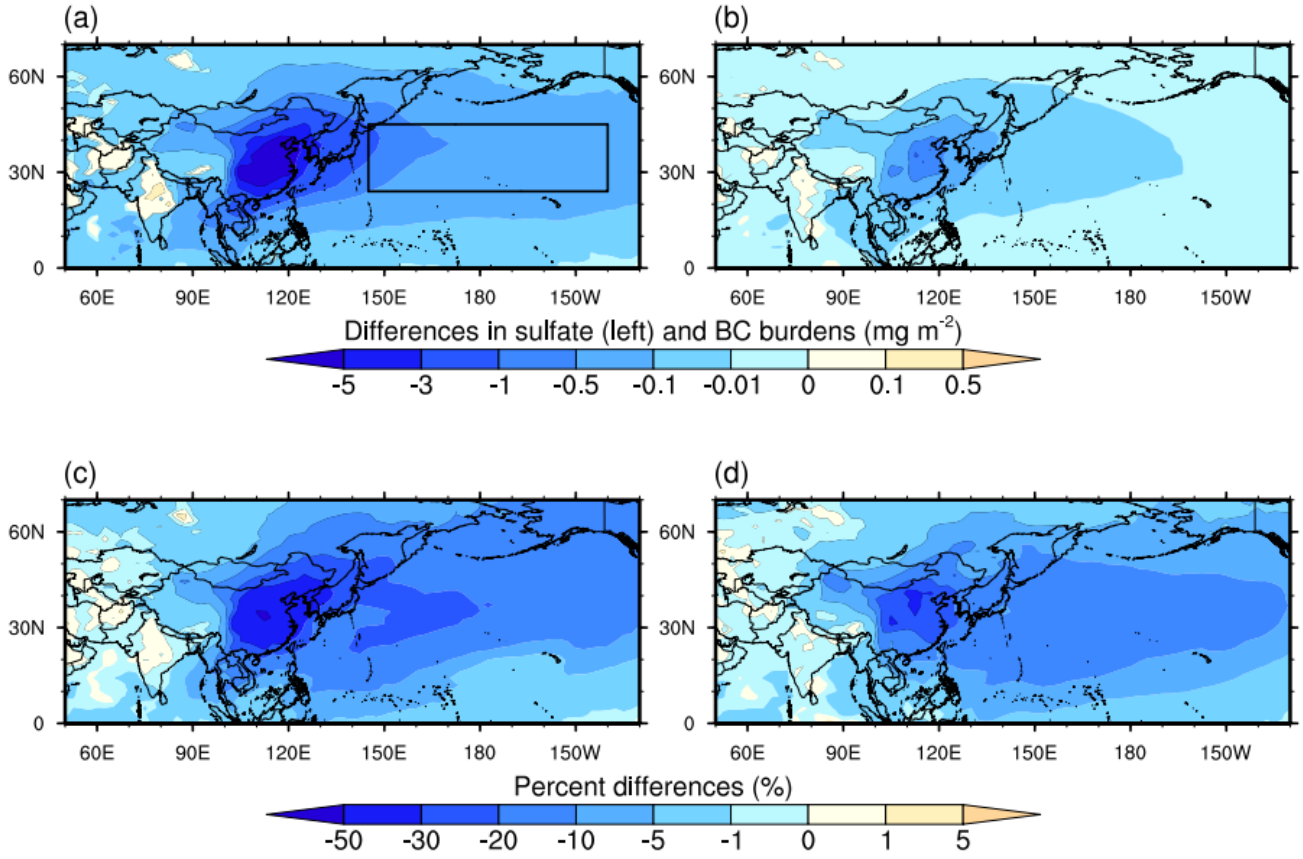

Figure 2. Change in particulate sulfate and BC burdens due to the emission variation in China between 2008 and 2016. (a-b) and (c-d) denote the mass (mg m^{-2}) and percent differences (%), respectively. The north Pacific region (24°−45° N, 145° E−140° W) is marked with the black box in Fig. 2a

635

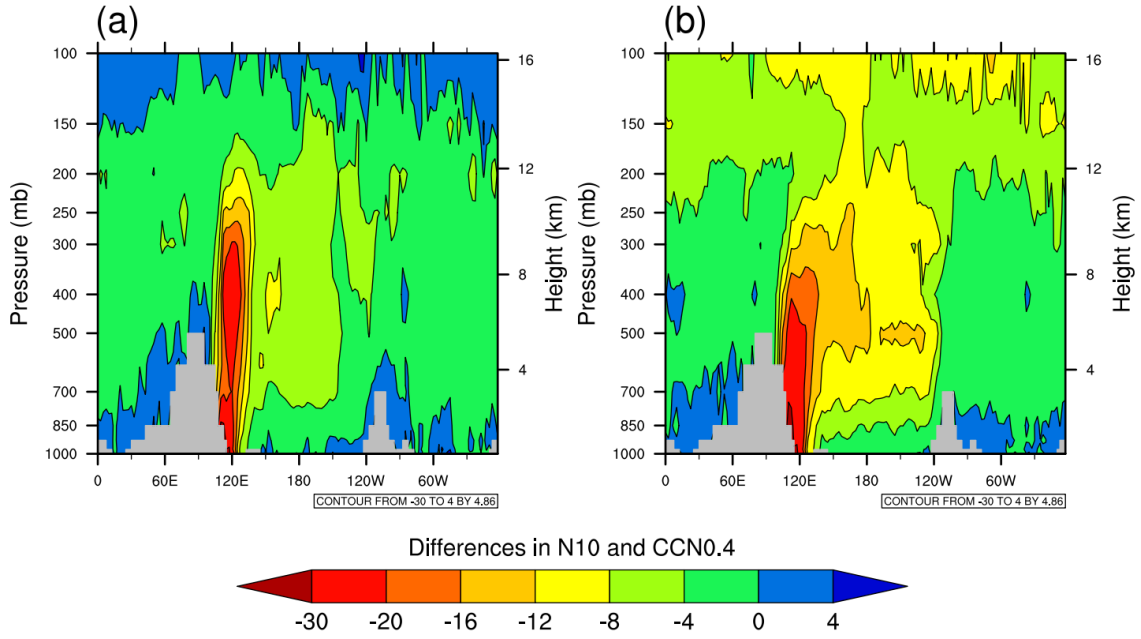

Figure 3. Pressure-longitude distribution of the annual-mean percent differences in the N10 and CCN0.4 along the latitude 35 ℃N due to the emission variation in China between 2008 and 2016

640

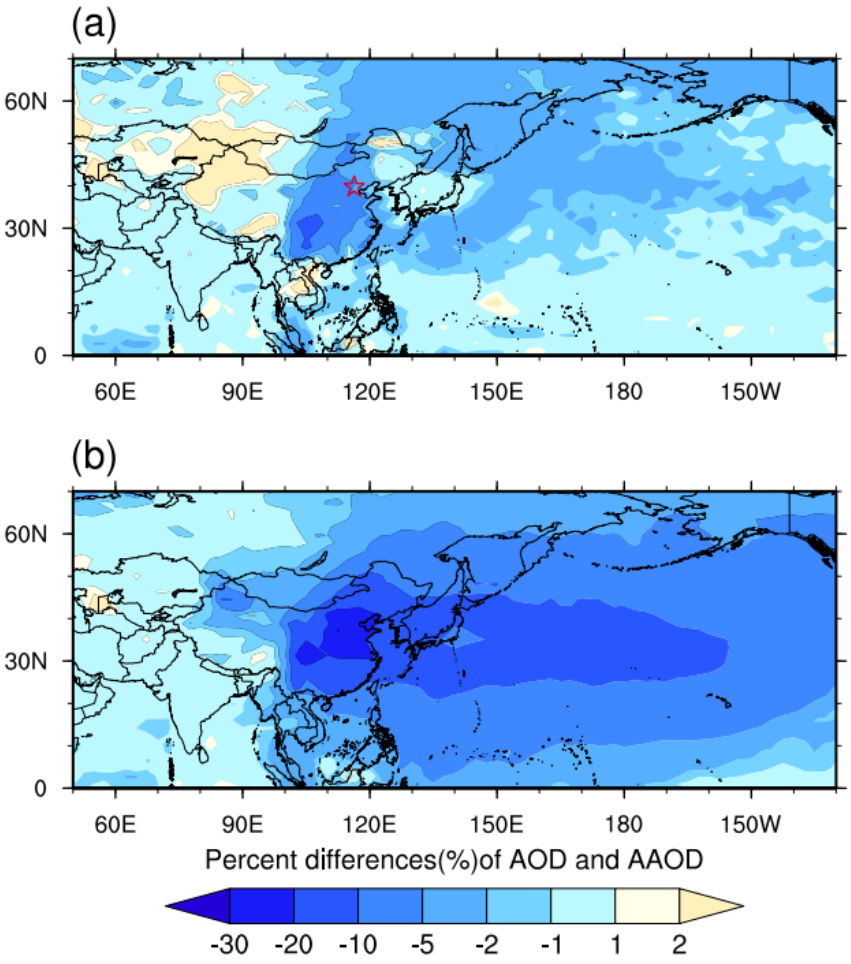

Figure 4. The changes (%) in AOD (a) and AAOD (b) due to variation in anthropogenic emissions in China between 2008 and 2016. The location of the AERONET site is marked with a red star.

645

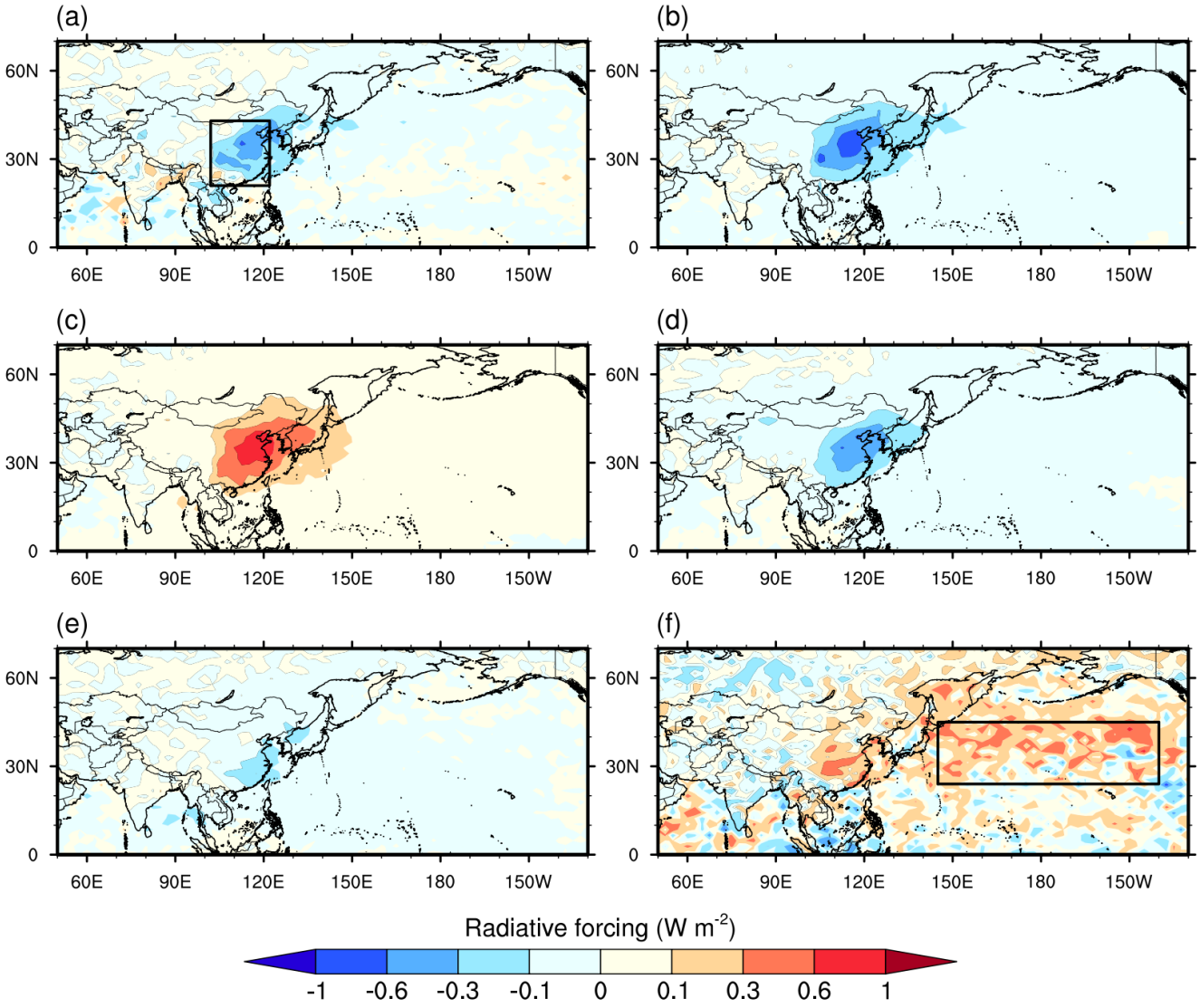

Figure 5. DRF from total aerosols (a), BC (b), sulfate (c), nitrate + ammonium (d), and OA + dust (e), and aerosol-induced CRF (f). Two regions of interest, East China and the north Pacific, are marked in Fig. 5a and 5f with black boxes.

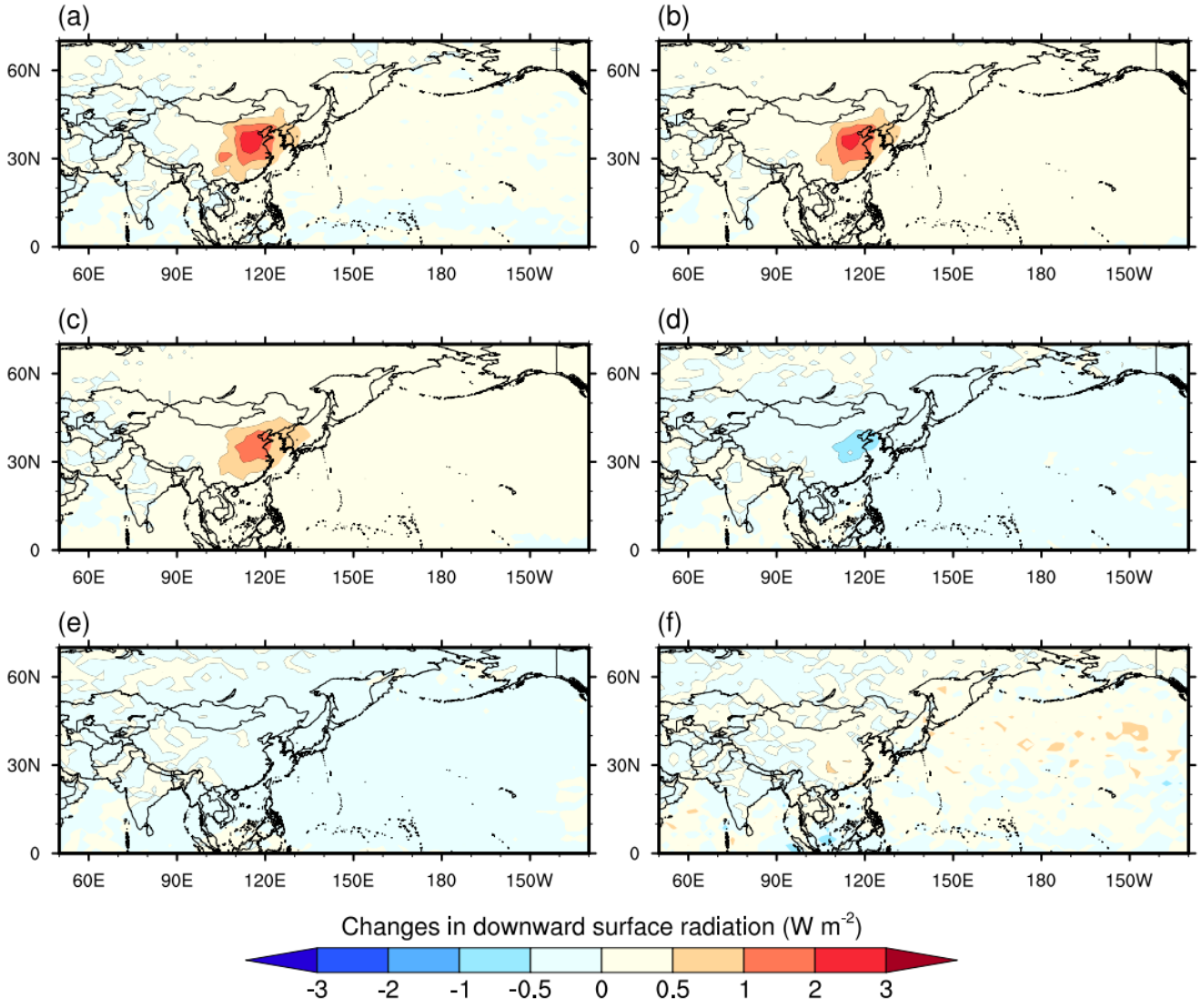

Figure 6. Changes in downward surface shortwave radiation over China and outflow regions between the emissions from 2008 and 2016 due to effects of all aerosols (a), BC (b), sulfate (c), nitrate + ammonium (d), OA + dust (e), and cloud albedo induced by aerosols (f). The positive values indicate the surface brightening and the negative surface dimming.

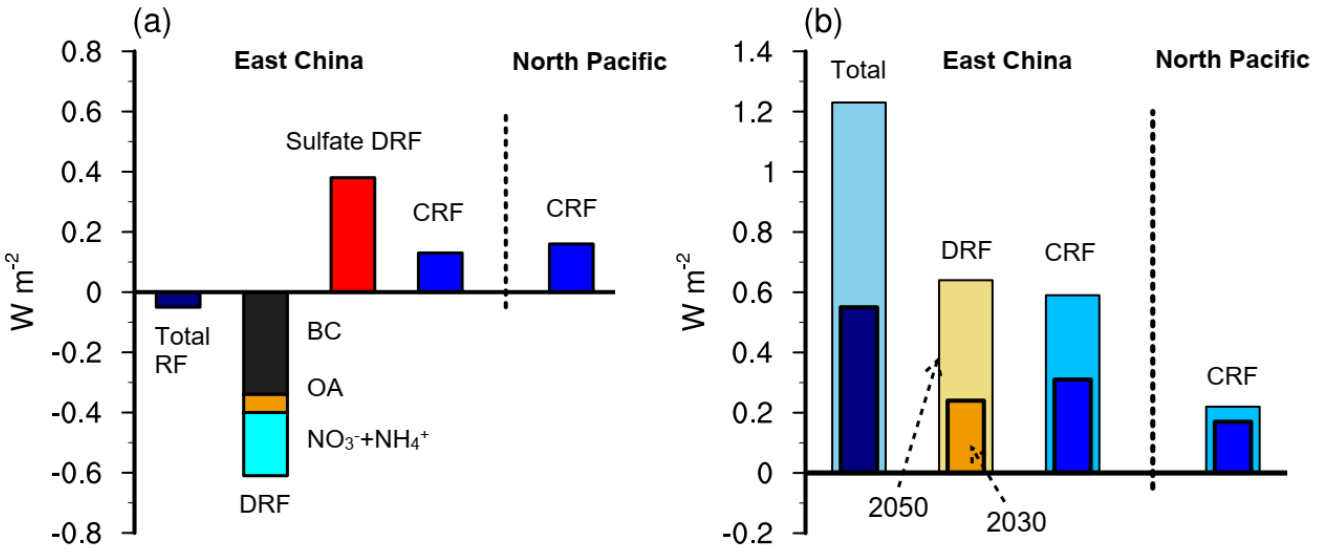

655 **Figure 7.** (a) Summary of total RF (sum of aerosol DRF and CRF), DRF for major aerosol components due to aerosol-radiation interactions, and aerosol effects on clouds (CRF) in East China and the north Pacific due to the changes in anthropogenic emissions between 2008 and 2016; (b) Aerosol DRF and CRF owing to projected anthropogenic emissions for 2030 and 2050 relative to 2016.